Clim Dyn (2012) 38:2275–2289
DOI 10.1007/s00382-011-1215-x

Vertical structure variability and equatorial waves during central Pacific and eastern Pacific El Niños in a coupled general circulation model

B. Dewitte · J. Choi · S.-I. An · S. Thual

Received: 24 January 2011 / Accepted: 3 October 2011 / Published online: 20 October 2011

Abstract Recent studies report that two types of El Niño events have been observed. One is the cold tongue El Niño or Eastern Pacific El Niño (EP El Niño), which is characterized by relatively large sea surface temperature (SST) anomalies in the eastern Pacific, and the other is the warm pool El Niño (a.k.a. 'Central Pacific El Niño' (CP El Niño) or 'El Niño Modoki'), in which SST anomalies are confined to the central Pacific. Here the vertical structure variability of the periods during EP and CP is investigated based on the GFDL_CM2.1 model in order to explain the difference in equatorial wave dynamics and associated negative feedback mechanisms. It is shown that the mean stratification in the vicinity of the thermocline of the central Pacific is reduced during CP El Niño, which favours the contribution of the gravest baroclinic mode relatively to the higher-order slower baroclinic mode. Energetic Kelvin and first-meridional Rossby wave are evidenced during the CP El Niño with distinctive amplitude and propagating characteristics according to their vertical structure (mostly first and second baroclinic modes). In particular, the first baroclinic mode during CP El Niño is associated to the ocean basin mode and participates to the recharge process during the whole El Niño cycle, whereas the second baroclinic mode is mostly driving the discharge process through the delayed oscillator mechanism. This may explain that the phase transition from warm to neutral/cold conditions during the CP El Niño is delayed and/or disrupted compared to the EP El Niño. Our results have implications for the interpretation of the variability during periods of high CP El Niño occurrence like the last decade.

B. Dewitte (✉) · S. Thual
LEGOS/IRD, 14 av. Edouard Belin,
31400 Toulouse, France
e-mail: bxd@legos.obs-mip.fr

J. Choi · S.-I. An
Yonsei University, Seoul, South Korea

1 Introduction

Many recent studies have showed that there exists more than one type of El Niño (or El Niño Southern Oscillation; ENSO) based on spatial distributions of SST (Larkin and Harrison 2005a, b; Ashok et al. 2007; Weng et al. 2007; Kao and Yu 2009; Kug et al. 2009; Yeh et al. 2009) or physically separated modes (Neelin et al. 1998; Jin et al. 2003; Bejarano and Jin 2008). So far, the ENSO has been categorized into two types of El Niño, the traditional Cold Tongue El Niño or Eastern Pacific El Niño (hereafter EP El Niño) that consists in SST anomaly developing and peaking in the eastern equatorial Pacific and the so-called Modoki El Niño (Ashok et al. 2007) or Central Pacific El Niño (Kao and Yu 2009; hereafter CP El Niño) that consists in SST anomaly developing and persisting in the central Pacific. Whereas the dynamics of the EP El Niño has been well documented (McPhaden et al. 1998), the observed increased occurrence of the CP El Niño during the last decades (Yeh et al. 2009) has led the community to investigate the mechanisms responsible for the triggering, development and decay of this different flavour of El Niño. Recent studies (Yu et al. 2010; Yu and Kim 2011) suggested an extratropical SLP forcing mechanism to explain the triggering of the CP El Niño whereas Yu and Kim (2010a) argued the decay of the CP El Niño is affected by the warm or cold phase of the EP El Niño. Kug et al. (2009) documented from the NCEP Reanalysis some aspects of the evolution of this kind of event, highlighting differences in the transition mechanism, namely the

recharge and discharge process of the equatorial heat content. In particular, they showed that the zonal advective feedback (i.e. zonal advection of mean SST by anomalous zonal currents) plays a crucial role in the development of SST anomalies associated with the CP El Niño, while the thermocline feedback is the key process during the EP El Niño. Kug et al. (2010) confirms these findings using a long-term model simulation that shows the major observed features of both types of El Niño, namely the GFDL model (Wittenberg et al. 2006). They further suggest that the frequency of occurrence of the CP El Niño event is related to the mean state of the tropical Pacific according to a two-way interaction process that makes the CP El Niño events rectifying on the mean warm pool, which in turn may favour the enhancement of anomalous zonal advection of mean temperature and so the development of the CP El Niño. Such mechanism was documented in more details in Choi et al. (2011) and is consistent with recent observed trend in both the warm pool (Cravatte et al. 2009) and the El Niño variability (Lee and McPhaden 2010). It is based on the observation that the discharge process during CP El Niño is weak and operates mainly through thermal damping (heat flux) rather than through equatorial wave dynamics like for the EP El Niño.

The reason for such difference in dynamics between CP and EP El Niño remains unclear. From a theoretical perspective, it is actually expected that, in a situation where the zonal advective feedback is dominant, the ENSO mode is destabilized by the gravest ocean basin mode, resulting in fast westward propagating SST anomalies (An and Jin 2001). If the zonal advection is a dominant process during the development of CP El Niño (Kug et al. 2009, 2010), the ocean basin mode may therefore be favoured (Jin and Neelin 1993; Kang et al. 2004), which may be propitious for the equilibrium between thermal damping and advection at basin scale. The difference of the recharge-discharge process between both types may actually results from a different dynamical adjustment that thereby modifies the heat flux equilibrium at the air-sea interface. This calls for investing the wave dynamics during the CP El Niño and the relevance of the negative feedbacks of ENSO (Neelin et al. 1998), namely the so-called delayed oscillator feedback (Schopf and Suarez 1988; Suarez and Schopf 1989) and the zonal advective feedback proposed by Picaut et al. (1996). Both are based on the delayed effect of reflected equatorial wave at the meridional boundaries on the vertical and zonal advection and are influential on the characteristics of the ENSO coupled instabilities (Jin and Neelin 1993; Neelin and Jin 1993; Dewitte 2000). As a preliminary step towards the evaluation of these feedbacks, it appears necessary to document the vertical structure and propagating characteristics of the equatorial waves during CP El Niño, which is central for ENSO dynamics.

This is the objective of this paper which can be seen as an extension of Kug et al. (2010) since it takes advantage of the long-term simulation of the GFDL model (Wittenberg et al. 2006) that simulates the major observed features of both types of El Niño, incorporating the distinctive patterns of each oceanic and atmospheric variable. Due to the time span of the simulation (500 years), statistical significance is achieved. Actually this model simulates CP and EP El Niño events that strikingly resemble two recent events representative of both type of El Niño events, namely the 1997/98 El Niño (EP El Niño) and the 2004/05 El Niño (CP El Niño). As an illustration, the Fig. 1 represents the time evolution of SST anomalies during these events both for the GFDL model composite and for the SODA reanalysis (Carton and Giese 2008). Model and Reanalysis data share many common features, which includes, the relative amplitude of the anomalies between El Niño types, the longitudinal location of peak SST anomalies and the seasonal evolution (see Kug et al. (2010) for further description of the ENSO composites of the GFDL model). Due to the compositing procedure (and model biases), the anomalies in the GFDL model are weaker than for the two observed events. Despite this limitation, the simulation offers the opportunity to investigate the vertical structure variability and associated equatorial wave during both type of El Niño, which can provide material for the interpretation of observed recent events. Yu and Kim (2010b) also report that the GFDL model is among the group of six models of the CMIP3 (World Climate Research Programme's Coupled Model Intercomparison Project phase 3) that best simulate both the EP and CP El Niños in terms of their intensity ratio.

The paper is organized as follows: The Sect. 2 describes the data sets and the method. The Sect. 3 is devoted to the analysis of the vertical structure variability whereas Sect. 4 documents the equatorial wave characteristics during both types of events. The Sect. 5 is a discussion followed by concluding remarks.

2 Data sets and method

2.1 The GFDL_CM2.1 model

The pre-industrial GFDL CM2.1 long-term simulation spanning 500 years is used. The ocean component is ocean model version 3.1 (Gnanadesikan et al. 2006; Griffies et al. 2005), which is based on Modular Ocean Model version 4 (MOM4) code. The resolution is 50 vertical levels and a $1^\circ \times 1^\circ$ horizontal grid telescoping to 1/3 meridional spacing near the equator. The vertical grid spacing is a constant 10 m over the top 220 m. The atmospheric component is the GFDL AM2p13 atmospheric model. The

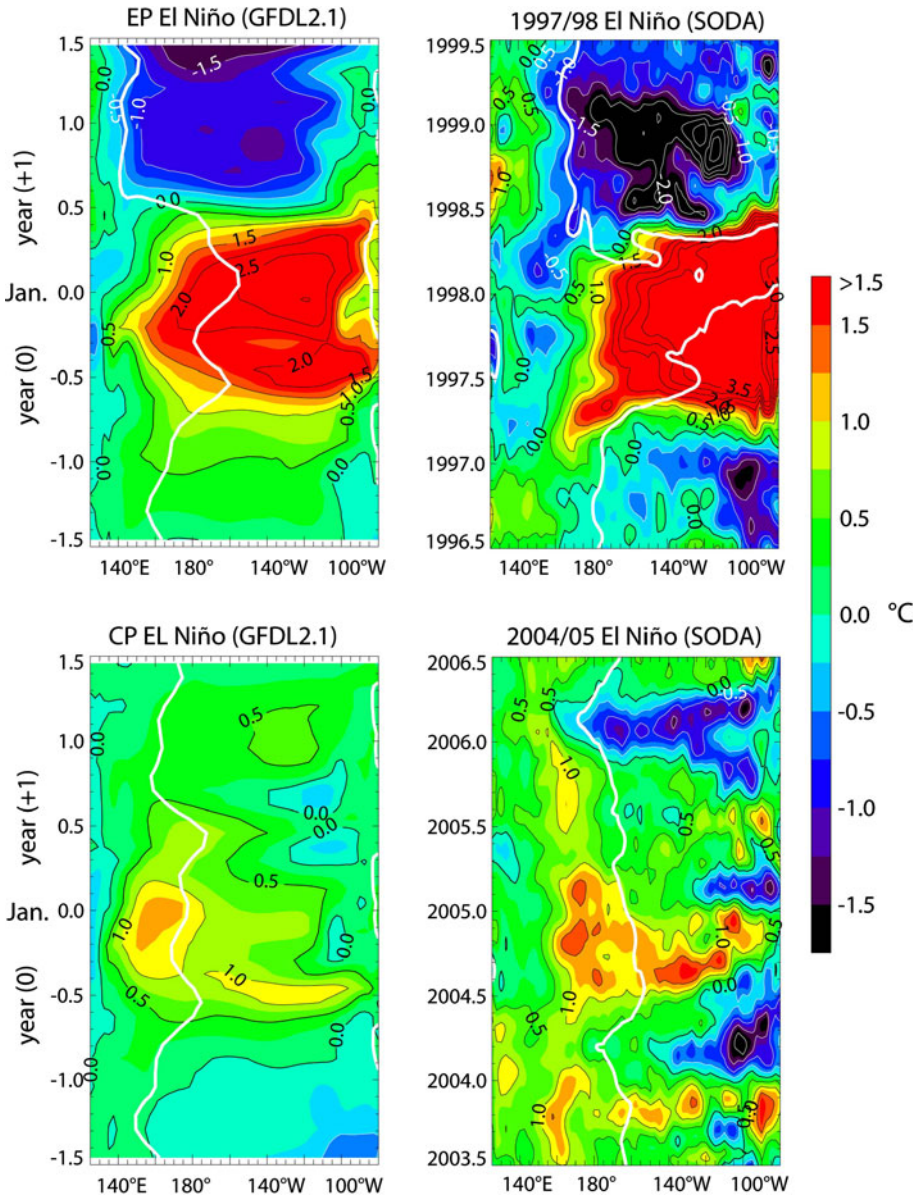

Fig. 1 Time longitude section of SST anomalies along the equator during the (*top*) 1997/1998 El Niño and the (*bottom*) 2004/2005 El Niño from (*right*) SODA and the (*left*) GFDL model. The *white thick line* indicates the position of the 28°C isotherm at the surface. Units are °C

resolution is 24 vertical levels, and 2° latitude by 2.5° longitude grid spacing. The dynamic core is based on a finite volume (Lin 2004). Air-sea fluxes are computed based on 1-h intervals. For a detailed model description, refer to Delworth et al. (2006) and Wittenberg et al. (2006). The data are available in the CMIP3 archives (https://www.esg.llnl.gov:8443/home/publicHomePage.do).

Following Kug et al. (2010), in order to define two-types of El Niño events, we use modified NINO3 and NINO4 SST indices because the climatological cold tongue extends farther west than observational data would suggest, and because ENSO variability is also shifted slightly to the west in the model. Wittenberg et al. (2006) noted that the simulated patterns of tropical Pacific SST, wind stress, and precipitation variability are displaced longitudinally by 20–30° west of the observed pattern. New indices are therefore defined NINO3m SST as the averaged SST over 170°–110°W, 5°S–5°N, and NINO4m SST as the averaged SST over 140°E–170°W, 5°S–5°N. Note that the area thus defined is shifted about 20° longitude to the west compared to the conventionally defined area. Based on the two indices, all El Niño events are initially selected when either of the two indices is greater than 0.5°C during NDJ. A total of 205 El Niño events were selected. We classified them as CP or as EP. El Niño events with a NINO4m SSTA greater than the NINO3m SSTA were considered CP, and those with a NINO3m SSTA greater than the NINO4m SSTA were labelled EP. We acknowledge that this division into only two groups is a limitation. Some events exhibiting similar magnitudes for NINO3m and NINO4m indices, though in

reality mixed, were still placed in one of the two groups. Based on our definitions, a total of 121 events were classified as CP El Niño events and 84 as EP El Niño events.

The reader is invited to refer to Kug et al. (2010) for details on how this procedure allows differentiating the two events in terms of dynamics and phenology.

2.2 Estimation of equatorial waves

A modal decomposition of the GFDL simulation was performed following a similar method than in Dewitte et al. (1999). As a first step, a vertical mode decomposition of the model mean stratification is sought at each longitude along the equator leading to the structure functions $F_n(x,z)$. Zonal currents $\{u(x,y,z,t)\}$ and pressure $\{p(x,y,z,t)\}$ anomalies are then estimated relative to the climatological seasonal cycle and these fields are projected on the vertical structure functions $F_n(x,z)$, leading to the baroclinic mode contributions to sea level and current anomalies. This implies computing the following quantity:

$$\langle q(x,y,z,t) \mid F_n(x,z)\rangle = \int_{H(x)}^{0} q(x,y,z,t)F_n(x,z)dz,$$

$H(x)$ being the ocean depth, and q being u or p. As a final step, the baroclinic modes are projected onto the theoretical meridional modes (Kelvin and Rossby modes) associated to the $F_n(x,z)$ to derive the Kelvin and Rossby waves coefficients. The reader is invited to refer to Dewitte et al. (1999) for more technical details. To derive the vertical modes, usually, the mean stratification over the entire model simulation is used. Here, to take into account that there is a change in mean density (e.g. mean stratification) at low frequency, we used the mean temperature and salinity profiles corresponding to the periods of high and low CP El Niño occurrence. Kug et al. (2010) defined a frequency index (number of occurrences) of both types of El Niño, defined by the number of events in a sliding 20-years period. They show that there is a strong negative correlation between the two indices, and that the periods of large CP (EP) occurrence corresponds to a warmer (cooler) SST in the central Pacific (their figure 13). Choi et al. (2011) further showed that the vertical temperature in the upper 300 m is also significantly different between the two periods (see also Fig. 2), which can be influential on the vertical mode functions. The vertical mode decomposition was therefore performed for the mean density corresponding to period of high (low) CP El Niño occurrence for the CP (EP) composite. The amplitudes of the Kelvin wave and the first-meridional mode of Rossby wave are then derived by projecting the pressure and zonal current baroclinic contributions onto the theoretical meridional modes.

The Kelvin (Rossby) wave contribution to thermocline anomalies was also estimated following Dewitte (2000), namely considering the vertical isotherm displacements at the depth of the mean thermocline and the hydrostatic approximation. For the Kelvin wave, it writes as follows:

$$\zeta_{AKn} = \frac{g}{N^2(x, z=\overline{h})}\frac{dF_n}{dz}(x, z=\overline{h})AK_n(x,y,t)$$

where AK_n is the Kelvin wave contribution to sea level anomalies for the nth baroclinic mode. $\overline{h}$ is the mean thermocline depth approximated as the depth of the 17°C isotherm of the mean temperature like in Choi et al. (2011). N^2 and F_n are the Brunt-Väisälä frequency and the nth vertical mode function respectively associated to the mean stratification during the periods of high and low CP El Niño occurrence. The estimation of the equatorial wave contribution to thermocline anomalies allows deriving the contribution of the Kelvin and Rossby wave (and baroclinic modes) to the warm water volume (hereafter WWV) anomaly defined as the zonal average (125°E–80°W, 5°S–5°N) of thermocline depth anomalies along the equator (Meinen and McPhaden 2000).

3 Vertical structure variability

The characteristics of the mean stratification control the baroclinic response of the equatorial Pacific Ocean to the wind forcing. In particular, a cooler mean state than normal in the vicinity of the mean thermocline (i.e. larger stratification) is generally associated locally to an increased variability of the higher-order modes (Dewitte et al. 2007, 2009) and vice versa. Figure 2a presents the change in mean temperature in the upper 300 m between the periods of high and low CP El Niño occurrence. Interestingly this pattern is similar to the residuals computed by a simple summation of El Niño and La Niña at their mature phase as well as the first empirical orthogonal function (EOF) pattern of the 20-years moving averaged equatorially-averaged subsurface ocean temperature, inferring that such pattern may result from the nonlinear rectification by a series of El Niño and La Niña (Choi et al. 2011). Both the depth and sharpness and intensity (i.e. magnitude of the Brunt-Väisälä frequency) of the thermocline are important to determine the baroclinic modes structure, and as so the influence of the subsurface variability onto SST. As seen in Fig. 2a, change in the thermocline depth is minimal, but its sharpness exhibit important changes, namely a warming at $\sim$100 m in the central Pacific and a cooling at $\sim$50 m in the eastern Pacific. In the central Pacific (170°E), this modifies the vertical structure of the thermocline as seen on the Brunt-Väisälä frequency in Fig. 2c. It indicates that the

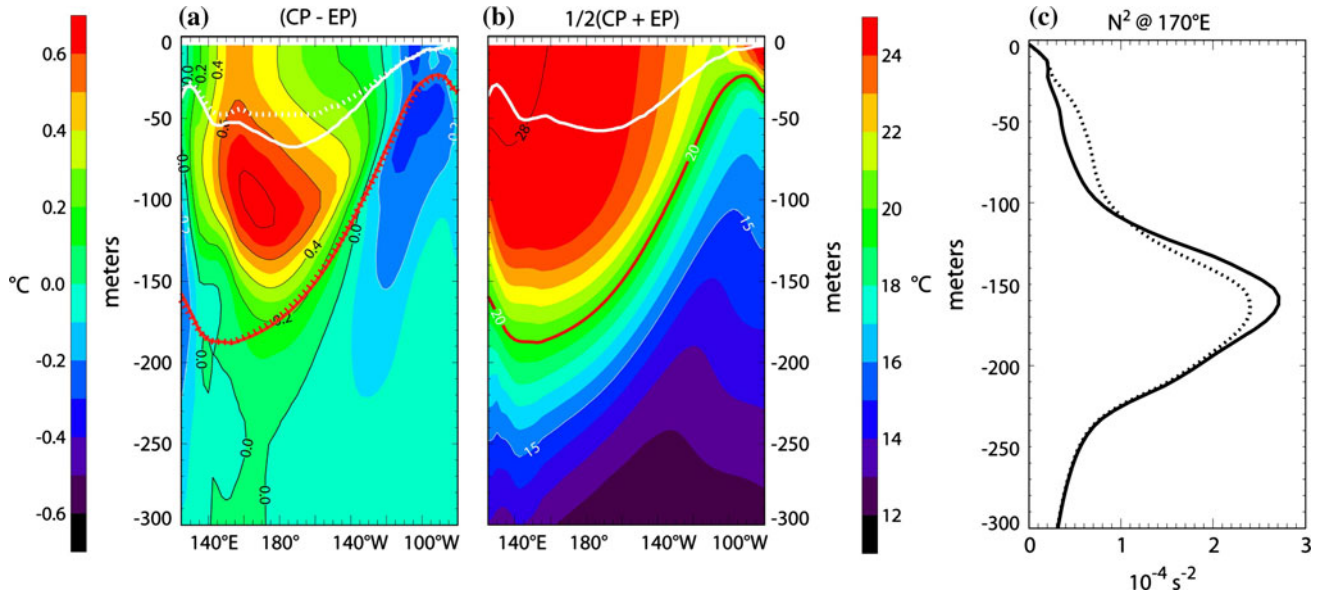

Fig. 2 Depth-longitude section of temperature along the equator for **a** the difference between periods of high CP El Niño occurrence and periods of high EP Niño occurrence and **b** for the whole period. The mean thermocline depth (20°C isotherm) is displayed on the first section in *white plain* (*red dotted*) *line* for the period of high CP (EP) El Niño occurrence. The mixed-layer depth for the period high CP (EP) El Niño occurrence is also displayed in *white plain* (*red dotted*) *line*. On the section of mean temperature, the 20°C isotherm depth is in *white thick line* where the mean mixed-layer depth is indicated by the *thick black line*. **c** Mean buoyancy profiles at 170°E for the periods of high EP Niño occurrence (*dotted line*) and of high CP occurrence (*plain line*)

thermocline is less diffuse during periods of high CP El Niño occurrence in the central Pacific, reflecting an increase in stratification of $\sim$20% at the thermocline depth compared to the periods of high EP El Niño occurrence (Fig. 2c). In the meantime stratification decreases from the surface to 100 m, reflecting that the Warm Pool is more homogeneous. The change in mixed-layer depth (MLD) is also indicative of the change in vertical structure variability between the two mean states. The MLD is deeper by about 20 m in the central Pacific between the periods of high and low CP El Niño occurrence [also shown in Choi et al. (2011)]. Note that change in MLD mostly impacts the high-order baroclinic modes ($n > 4$), which can account for the variability trapped in the surface layer due to their fine vertical scales of variability.

Change in stratification can be quantified through the estimation of the wind projection coefficient (Lighthill 1969). The Fig. 3 presents the difference in the wind projection between periods of high CP El Niño occurrence and low CP El Niño occurrence. It indicates that, whereas the difference in P_1 is hardly changed (slight increase), those in P_n for higher-order modes decrease monotonically with the mode order, reaching variation as large as 60% for the fifth baroclinic mode in the central Pacific. Note that the first two baroclinic modes are the most relevant for documenting equatorial waves because they are the ones that exhibit clear propagating characteristics (because they dissipate the least). In order to be interpretable, high-order modes have to be considered as a summed-up contribution, and as so can be considered as the variability that is trapped in the surface layer and that is forced mostly locally (Dewitte et al. 1999). Note that although changes in P_n are the largest for the high-order modes, their summed-up contribution to zonal current anomalies may not change that drastically because the projection of zonal current anomalies on a particular baroclinic mode can results in either westward or eastward surface currents (depending on the vertical structure of the zonal current anomalies), resulting in a compensating effect between modes.

The Fig. 3 suggests that the mean stratification tends to disfavour the higher-order mode contributions to the variability during CP El Niño periods as compared to EP El Niño periods. Although the thermocline is less diffuse during CP El Niño periods, the Warm Pool is more

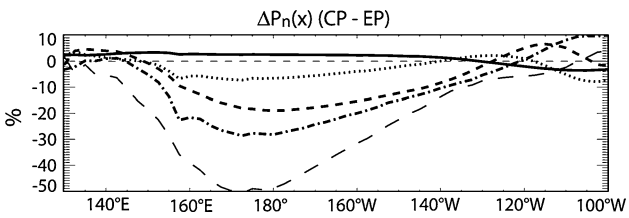

Fig. 3 Change in wind projection coefficient (in %) between CP and EP El Niño periods as a function of longitude. The *plain* (*dotted*) *line* is for the first (second) baroclinic mode. The *thick dashed* (*dotted-dashed*) *line* is for the third (fourth) baroclinic mode. The *thin dashed line* is for the fifth baroclinic mode

homogeneous (cf Fig. 2c) which overall leads to a reduced projection of wind stress forcing onto the higher baroclinic modes. Dynamically, this implies a tendency towards ENSO related coupled instabilities having a faster propagating speed (Dewitte 2000). The enhancement of the first baroclinic mode relatively to the higher-order mode favours an unstable mode having a fast westward propagation and tends to increase the ENSO frequency (Dewitte 2000). This is because the suppression of higher-order modes promotes the relative contribution of the zonal advection feedback, which destabilizes Rossby waves. This point will be got back to in Sect. 4.

As mentioned above, the inspection of the P_n is however not sufficient to fully diagnose the relative contribution of the baroclinic modes to the variability. Due to difference in variability characteristics between the two events (Kug et al. 2009), it is necessary to analyse the actual projection of the variability onto the vertical mode functions. The Fig. 4 provides such diagnostics for the zonal current anomalies during the different phases of the events for the EP El Niño composite. The peak phase corresponds to the mean centred in January of year 1 within a 5-months window (±2 months), the developing (decaying) phase is centered 6 months before (after) the peak phase. Due to difference in amplitude of the two type of El Niño, the variability was divided by the NINO3m SST and NINO4m SST anomaly index in Dec (Year 0) –Jan–Feb (Year 1) respectively. In order to derive the contribution of the summed-up contribution of the high-order modes ($n > 4$), relevant to the Ekman dynamics, a simple frictional equation forced by $\vec{\tau}_f = \vec{\tau}\left(\frac{1}{h_{mix}} - \sum_{i=1}^{3} P_i\right)$ is considered following Blumenthal and Cane (1989) (P_i being the wind projection coefficient for the baroclinic mode i and h_{mix} is the mixed-layer depth). The later represents the share of the momentum flux that does not project on the gravest baroclinic modes (here, the first three baroclinic modes). This leads to the estimation of zonal Ekman currents as:

$$u_{\mathrm{Ekm}} = \frac{r_s\tau_x + \beta y\tau_y}{\rho_0(r_s^2 + \beta^2 y^2)}\left(\frac{1}{h_{\mathrm{mix}}} - \sum_{n=1}^{3} P_n\right)$$

where ρ_0 is the mean density, r_s is a damping rate coefficient of 1.5 days^{-1} and (τ_x, τ_y) is the zonal and meridional wind stress anomalies.

The evolution of the total surface current anomaly clearly illustrates the zonal advection process during EP El Niño, namely eastward zonal current anomalies in the vicinity of the eastern edge of the warm pool during the developing and peak phases of the event. The decaying phase is associated to strong westward surface currents bringing back the warm pool westward. In terms of projection onto the baroclinic modes, the Fig. 4 indicates that each mode has a different evolution, with the first mode participating earlier than the other modes to the negative feedback (westward equatorial current during the peak phase). The strong reversal towards La Niña condition is due to the contribution of modes 2 and 3 that exhibit intense westward current during the decaying phase. Ekman current anomalies have a westerly component in the central Pacific during all phases, of which centre seems to move eastward. An interesting aspect of the vertical mode distribution is that the zonal current variability during the reversal towards La Niña conditions takes place mostly north of the equator through the second baroclinic mode. This is consistent with the geostrophic adjustment consecutive to the discharge process (or ENSO-related meridional mass transport) being larger in the Northern Hemisphere than in the Southern Hemisphere during EP El Niño (e.g. Kug et al. 2003). This is in contrast with the CP El Niño as will be seen (Fig. 6).

Figure 5 presents the similar analysis to Fig. 4 but for the CP El Niño composite. It indicates that the CP El Niño has a different vertical mode distribution in terms of zonal current anomalies than the EP El Niño, reflecting the differences in time evolution. First of all, eastward zonal current anomalies in the central-western Pacific during the developing phase mostly project onto the second baroclinic mode. Except during this phase, the baroclinic zonal circulation is dominated by westward current anomalies in the central and eastern Pacific, which actually lead to the cooling SST tendency through the cold temperature advection. The warming tendency is maintained through the eastward Ekman current anomalies in the far western Pacific during all phases. Interestingly, the negative feedback associated to the westward current anomalies take place during the peak phase of the event, which is in contrast with the EP El Niño composite. These westward current anomalies project mostly onto the first two baroclinic modes and peak south of the equator. Note also the westward current anomalies associated to the Ekman component in the eastern Pacific is consistent with the increase in trade winds during the period of high CP El Niño occurrence (Choi et al. 2011).

In order to determine how the differences between El Niño types reflect in the dynamic height, the Fig. 6 displays the results of the vertical mode decomposition in terms of sea level anomaly contribution. Only the first two baroclinic modes are presented because they are the most relevant for the geostrophic basin scale adjustment associated to wave dynamics. The results indicate that, whereas the sea level pattern during EP El Niño is characterized by a zonal seesaw reflecting the forcing of energetic eastern Pacific Kelvin and western Pacific Rossby waves, the sea level pattern during CP El Niño tends to have has a basin-scale structure with positive sea level anomalies over most of the equatorial Pacific (peaking in the central and western

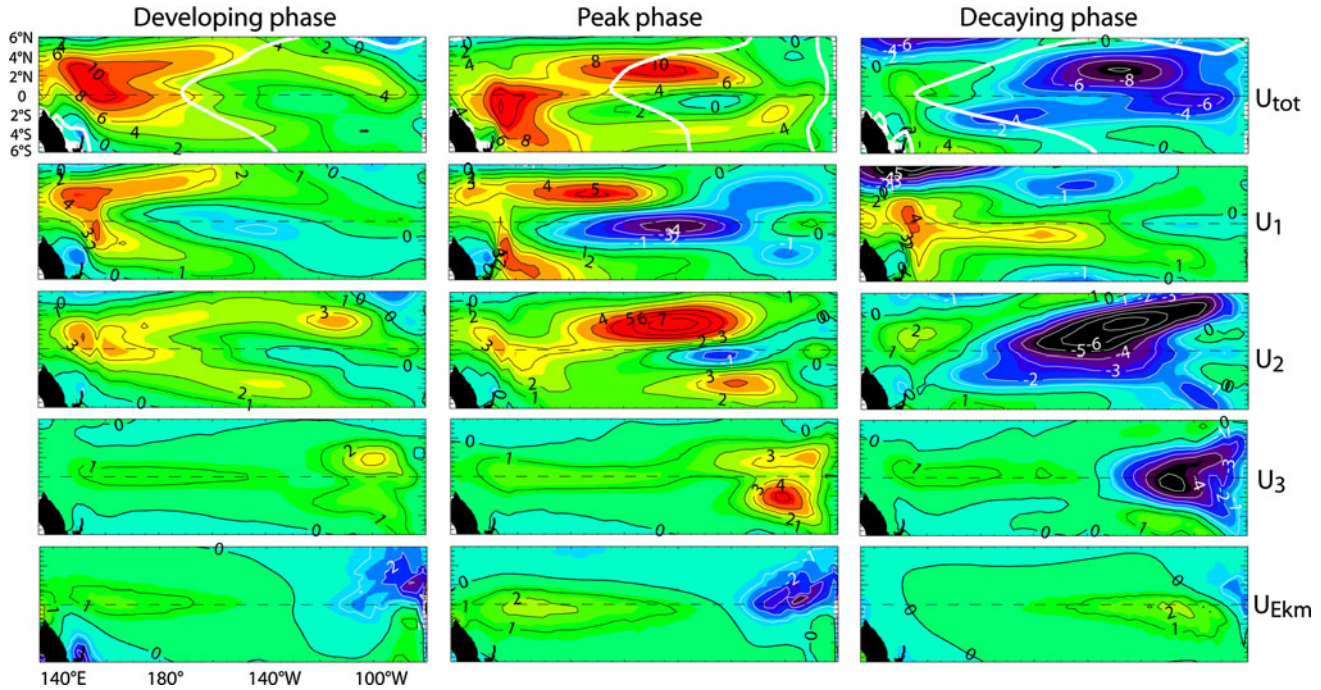

Fig. 4 Mean surface zonal current anomalies for EP El Niño during the developing phase (year -0.5 ± 2 months), the peak–peak phase (year 0 ± 2 months) and the decaying phase (year 0.5 ± 2 months). From *top* to *bottom*: total, first baroclinic mode contribution, second baroclinic mode contribution, third baroclinic mode contribution and Ekman current contribution. In order to compare with the equivalent maps for the CP El Niño (Fig. 5), the maps are divided by the NINO3m SST index in Dec–Jan–Feb (Year 0), i.e. 2.06°C. Units are therefore cms^{-1} 0.48°C^{-1}. The *white thick line* on the total surface current anomaly maps represents the mean position of the 28°C isotherm for SST during the different phases

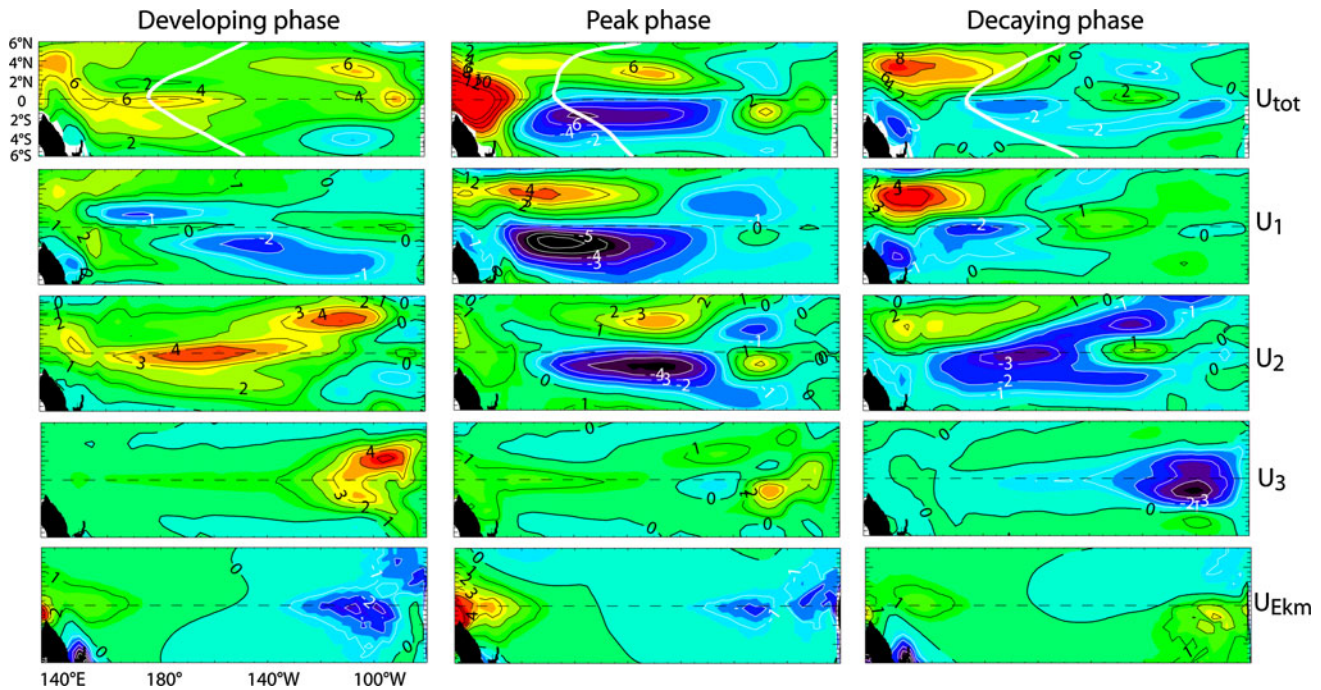

Fig. 5 Same as figure 5 but for the CP El Niño. The maps have been divided by the NINO4m SST index in Dec–Jan–Feb (Year 0), i.e. 0.85°C

Pacific and resembling the ocean basin mode (Jin and Neelin 1993)) during the developing and peaking phases. The differences between El Niño types are also evident for the meridional structure of the sea level anomalies, mostly symmetrical towards to the equator for the EP El Niño for all phases, and anti-symmetrical for the CP El Niño during

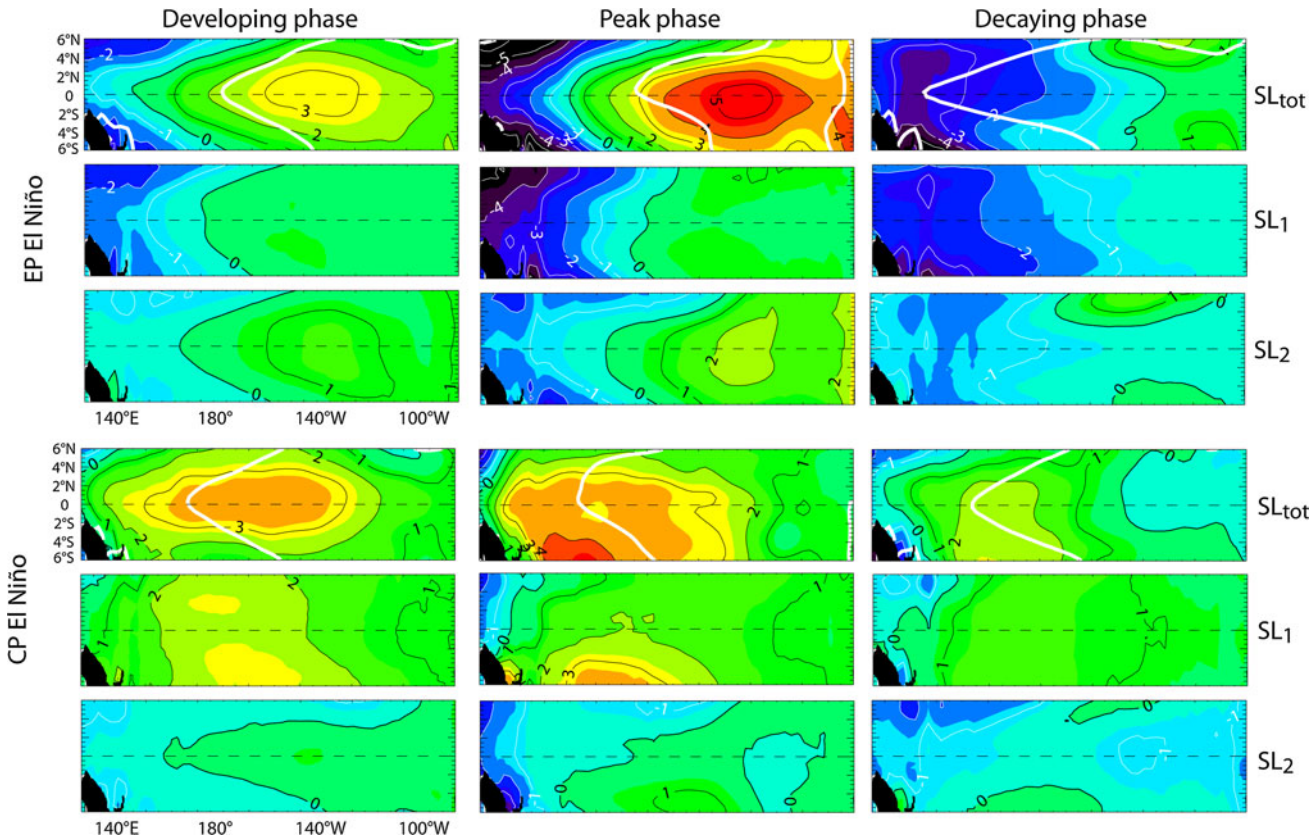

Fig. 6 Mean sea level anomalies for (*top panels*) EP El Niño and (*bottom panels*) CP El Niño during the developing phase (year -0.5 ± 2 months), the peak–peak phase (year 0 ± 2 months) and the decaying phase (year 0.5 ± 2 months). From *top to bottom*: total, first baroclinic mode contribution and second baroclinic mode contribution. The maps are divided by the NINO3m SST index in Dec–Jan–Feb (Year 0), i.e. 2.06°C for the EP El Niño and by the NINO4m SST index in Dec–Jan–Feb (Year 0), i.e. 0.85°C for the CP El Niño. Units are therefore cm $0.48°C^{-1}$ (cm $1.18°C^{-1}$) for EP (CP) El Niño. The *white thick line* on the total sea level anomaly maps represents the mean position of the 28°C isotherm for SST during the different phases

the peaking and decaying phases, with larger anomalies in the South Hemisphere than in the Northern Hemisphere. This is consistent with the larger zonal current variability resulted from geostrophic adjustment in the Southern Hemisphere during CP El Niño.

The vertical mode decomposition confirms the almost in-phase relationship between mode 1 and 2 and the dominance of mode 2 at the peak phase for the EP El Niño. On the other hand, for the CP El Niño, the baroclinic mode contributions to sea level anomalies have a more contrasted characteristic, namely a positive basin scale and stationary sea level anomaly for mode 1 that dominates, and an evolving pattern towards basin scale negative anomaly for mode 2, which reflects the cooling effect of mode 2. The differences in projection of the sea level anomaly evolution onto the baroclinic mode reflect the difference in recharge-discharge process during the two types of El Niño. In particular, the rather large zonal extent of the sea level positive anomaly during CP El Niño of the first baroclinic mode (which traduces a specific forcing characteristic) will not favour the delayed oscillator feedback process because energetic upwelling Rossby wave are not forced during the developing and peak phases of the event. The negative feedback process can operate through the second baroclinic mode which exhibit a zonal seesaw pattern as in the case of the EP El Niño. However its effectiveness may be reduced due to both the weaker contribution of mode 2 and its larger dissipation (slower phase speed). This is in contrast with what happens during EP El Niño event. This will be further discussed in the last section.

4 Equatorial wave contributions

Considering the above differences in baroclinicity during the two types of event, it is now interesting to document the propagating characteristics of the equatorial waves, the Kelvin and first-meridional Rossby waves, during both type of event. Whereas equatorial wave characteristics have been well documented for EP El Niño-type, in particular during the 1997/98 El Niño (Boulanger and Menkes 1999; Dewitte et al. 2003), the investigation of CP El Niño-

type in terms of equatorial wave are very few (McPhaden 2004). The GFDL composite offers the opportunity to reveal statistically significant features, which can be then used to interpret observed events. As a benchmark, we present the results of the horizontal mode decomposition for the EP El Niño (Fig. 7). Results of Fig. 7 are consistent with an earlier study that documented the wave sequence according to the first two baroclinic mode during the 1997/1998 El Niño (Dewitte et al. 2003), indicating that the characteristics of equatorial waves associated with EP El Nino in the GFDL model are consistent with counterparts of the observations. In particular, the EP El Niño is characterized by a similar contribution and a quasi in-phase relationship of the first and second baroclinic modes Kelvin and Rossby waves, with the second baroclinic mode Kelvin wave growing during the mature phase and leading to the sharp reversal towards cool conditions through the reflection into Rossby wave at the eastern boundary [see Dewitte et al. (2003)].

We now document the wave sequence during the CP El Niño (Fig. 8). The developing phase is somewhat similar to the one of the EP El Niño as the two downwelling (i.e. positive) Kelvin modes work together to intensify SST anomaly in the central Pacific, with however a dominant contribution from mode 1 instead of mode 2. The marked difference with the EP El Niño (Fig. 7) is the positive sign of the Kelvin wave of the first baroclinic mode during the decay phase, especially between Year 0 and Year +1. Therefore during CP events the first baroclinic mode is mostly associated to downwelling (i.e. positive) Kelvin wave over the whole cycle, which veils the delayed oscillator (e.g. recharge-discharge) negative feedback process. Whereas the first baroclinic mode is mostly associated to downwelling (i.e. positive) Kelvin wave over the whole cycle, the second baroclinic mode is dominated by the upwelling (i.e. negative) Kelvin waves during the peak and decaying phases, which may damp SST anomalies in the central and eastern Pacific through vertical advection. However in the decaying phase, the contributions by the two Kelvin modes are opposite so the effects may be compensated to each other. Another interesting feature is the limited zonal extension of the Kelvin and Rossby waves for the first baroclinic mode with peak variability in the central Pacific. In particular, the first vertical mode resembles the ocean basin mode (Jin and Neelin 1993; Neelin and Jin 1993; Kang et al. 2004) such that the maximum appears at the centre of the basin and the minimums (nodes) are located at the boundaries. This tends to increase the contribution of the zonal advective feedback (more intense in the central Pacific) with respect to the thermocline feedback (more intense in the eastern Pacific) in relation with equatorial wave variability. Therefore in some sense, the CP El Niño may be related to the excitement of the ocean basin mode, which is destabilized by the zonal advective feedback. Propagating characteristics of the Kelvin wave also suggest more intense modal dispersion in the eastern Pacific than during the EP El Niño. Note for instance the sharp decay (amplification) of the downwelling (upwelling) Kelvin wave amplitude of baroclinic mode 1 (2) at ~120°W. This is consistent with the fact that the east–west contrast of stratification is more intense during CP El Niño than during EP El Niño because the

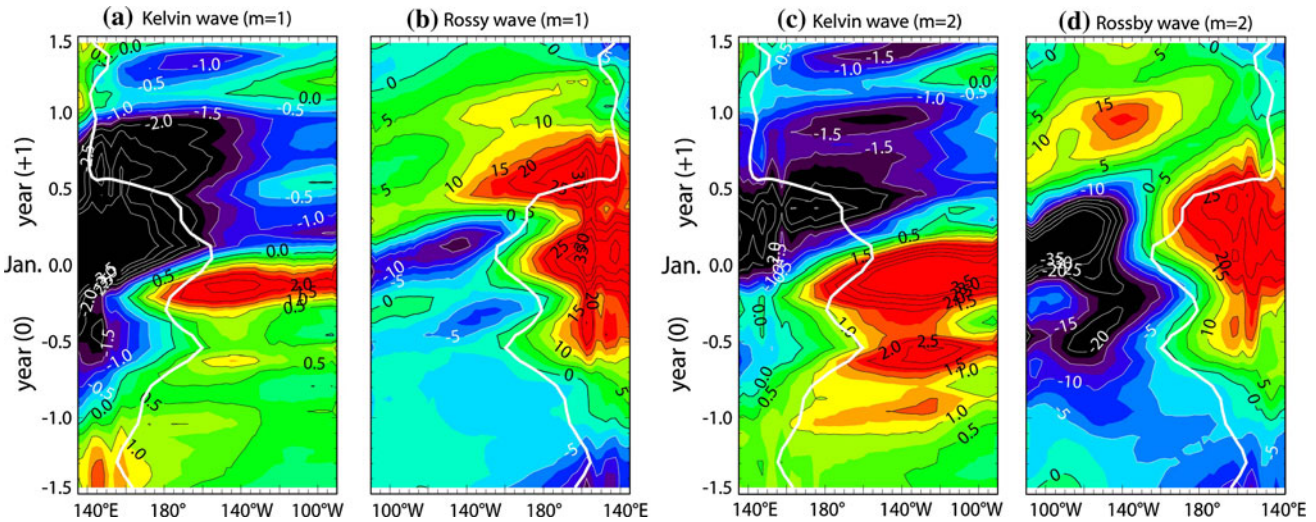

Fig. 7 Time-longitude section of the equatorial Kelvin wave (AK in cm) and the first meridional Rossby wave (R1 in cms^{-1}) along the equator for the (*left*) first and (*right*) second baroclinic modes during EP El Niño event. R1 is displayed in reverse from 90°W to 135°E to visualize wave reflections at eastern boundaries. Because R1 accounts for currents and AK for sea level, they have opposite sign near the boundaries. Contour intervals are 0.5 cm for AK and 5 cms^{-1} for R1. The *thick white line* represents the position of the 28°C isotherm for SST

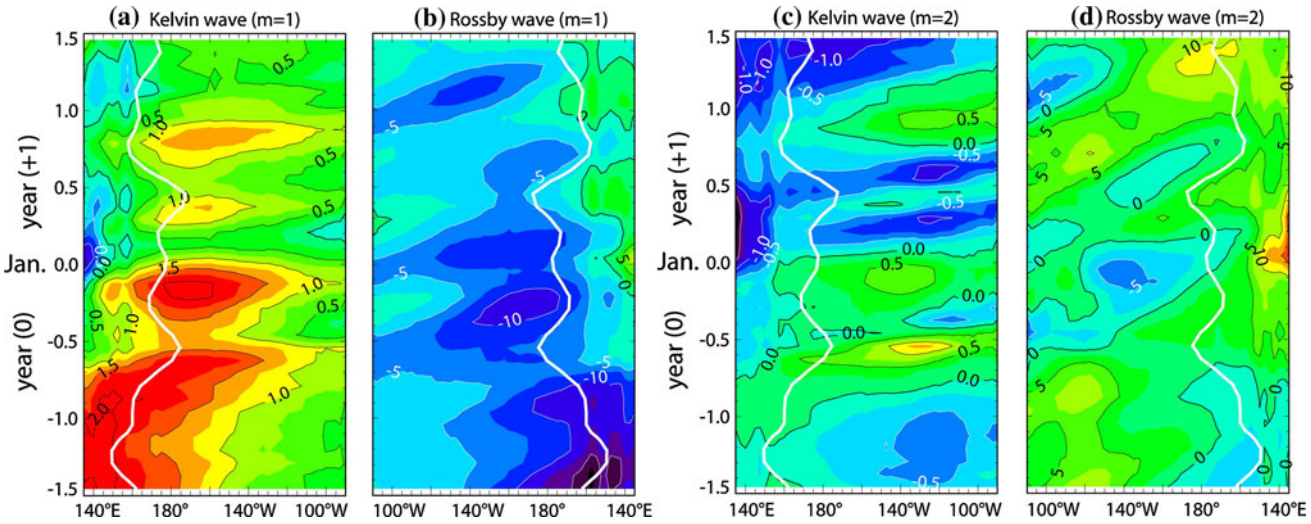

Fig. 8 Same as Fig. 7 but for the CP El Niño event

mean thermocline slope is hardly modified during the CP El Niño. Furthermore, as mentioned in An and Jin (2000), because the natural frequency of the ocean basin mode is higher than the frequency of the ocean basin adjustment mode, a shorter period of oscillation would be expected for CP El Niño as compared to EP El Niño. Like for the EP El Niño, the displacement of the eastern edge of the warm pool mimics the pulses of downwelling Kelvin wave. However the downwelling Kelvin wave slightly leads the displacement of the warm pool edge, possibly because of the delayed SST response to the vertical thermal advection (Zelle et al. 2004).

The Fig. 9 further illustrates the peculiarities of the Kevin wave according to the baroclinic modes during CP El Niño contrasting with the EP El Niño. For the CP El Niño in particular, it is obvious that only the second baroclinic mode has a cooling effect during the decaying phase. Such cooling effect is all the more important in the eastern Pacific as the mean thermocline is shallower than during EP El Niño. On the other hand, in the central Pacific, since the thermocline is deeper than normal, the effectiveness of the upwelling Kelvin/Rossby wave is limited.

5 Discussion and conclusions

A long-term simulation of the GFDL_CM2.1 model was used to document the variability characteristics of the CP and EP El Niño in terms of equatorial wave. It is shown that, despite a weaker variability than the EP El Niño, the CP El Niño is associated to energetic first and second baroclinic mode Kelvin and Rossby waves. Whereas for the first baroclinic mode Kelvin wave have the maximum amplitude at the centre of the basin and the minimum amplitude (nodes) at the boundaries, resembling the ocean basin mode (Jin and Neelin 1993; Neelin and Jin 1993; Kang et al. 2004), the second baroclinic mode Kelvin wave exhibits clearer free propagating characteristics resembling the ocean adjustment mode of the EP El Niño (Jin 1997), In particular, energetic upwelling Kelvin waves of the second baroclinic mode are generated during the decaying phase of the event, which maintains the east–west mean SST contrast across the Pacific, auspicious for the enhancement/maintenance of the effectiveness of the zonal advective feedback. This may explain the persistence/maintenance of warm SST anomalies in the western Pacific during CP El Niño. It also indicates that the reflective advective feedback process proposed by Picaut et al. (1996) cannot be effective during CP El Niño events, basically because the first baroclinic mode downwelling Kelvin waves has a weak amplitude near the eastern boundary and because the eastern edge of the warm pool remains in the central Pacific. Similarly the delayed oscillator is not operating during CP El Niño for the first baroclinic mode in the GFDL model which may be attributed to the western most position of the wind variability (Kug et al. 2010; cf. Fig. 11). The wind stress forcing located near the western boundary does not allow for accumulation of momentum forcing towards the upwelling Rossby wave. In particular wave reflection at the western boundary appears to be weak (Fig. 8a, b), preventing negative feedback through the reflected upwelling Kelvin wave. These differences in negative feedback processes associated to wave dynamics between El Niño types suggest that the recharge-discharge process (Jin 1997) is operating differently during the two type of El Niño. As a consistency check of this latter statement, the WWV anomaly associated to the Kelvin and

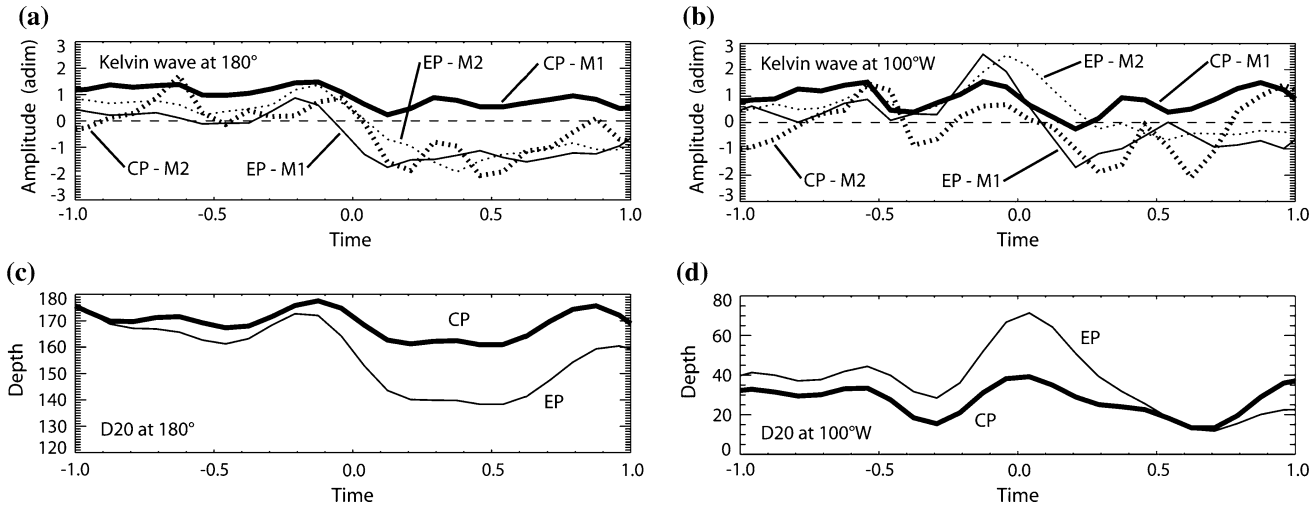

Fig. 9 Time evolution of the **a**, **b** Kelvin wave amplitude and **c**, **d** thermocline depth (20°C isotherm depth) at 180° and 100°W. *Thick* (*thin*) *lines* are for the CP (EP) El Niño. *Dotted* (*plain*) *lines* are for the second (first) baroclinic modes. Kelvin wave amplitude has been adimensionalized by its variability (RMS) between −0.5 and +0.5 years

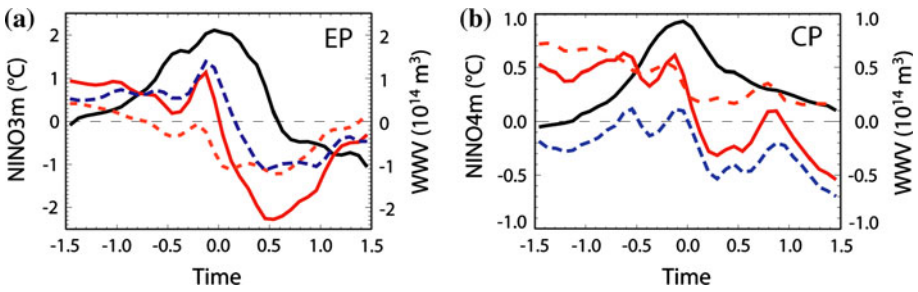

Fig. 10 Evolution of the **a** NINO3m and **b** NINO4m SST indices (*thick black lines*) and Warm Water Volume (125°E–80°W; 5°S–5°N) anomaly during the EP and CP El Niños. The Warm Water Volume considers the contribution of the Kelvin and first-meridional Rossby wave of the first baroclinic mode (*red dashed line*), of the second baroclinic mode (*blue dashed line*) and the summed-up contribution of the first two modes (*thick full red line*)

first-meridional Rossby waves was estimated (see Sect. 2). Its evolution during the two types of El Niño is presented in Fig. 10. Besides differences in amplitude (reflecting differences in the magnitude of the events), the WWV has a comparable evolution for both type of event, namely a recharge prior to the maximum SST anomaly and a discharge later on. However for the CP El Niño, the decrease of the WWV anomaly is relatively weaker than for the EP El Niño. The most striking difference between CP and EP El Niño events is mainly in the role of the baroclinic modes: For the EP El Niño, the WWV anomaly associated to the first and second baroclinic modes has a comparable evolution and amplitude. However for the CP El Niño, the WWV anomaly of the first baroclinic mode is associated to a recharge process during almost the whole cycle while the WWV anomaly of the second baroclinic mode is associated to the discharge process after the peak SST anomaly. This is consistent with the Kelvin wave decomposition of the CP El Niño, which indicates that the first baroclinic mode is associated to the warming of SST through downwelling Kelvin wave, whereas the second baroclinic modes tends to be associated to the cooling of SST (in particular in the eastern equatorial Pacific) through upwelling Kelvin wave that are all the more efficient that the mean thermocline is shallower during periods of CP El Niño occurrence.

The peculiarities of the Kelvin waves during the CP El Niño event are more than likely resulting from the characteristics of the zonal wind stress forcing, although they could also result from non-linear processes such as modal dispersion. In particular since the thermocline remains shallow in the east during the CP El Niño and because wave amplitude is weaker than during the EP El Niño, the modal dispersion process associated to the east–west zonal contrast in stratification can be operating effectively (Busalacchi and Cane 1988). This is consistent with the sharp decay of the downwelling Kelvin wave of the first baroclinic mode around ∼120°W (Fig. 8a) and the relative

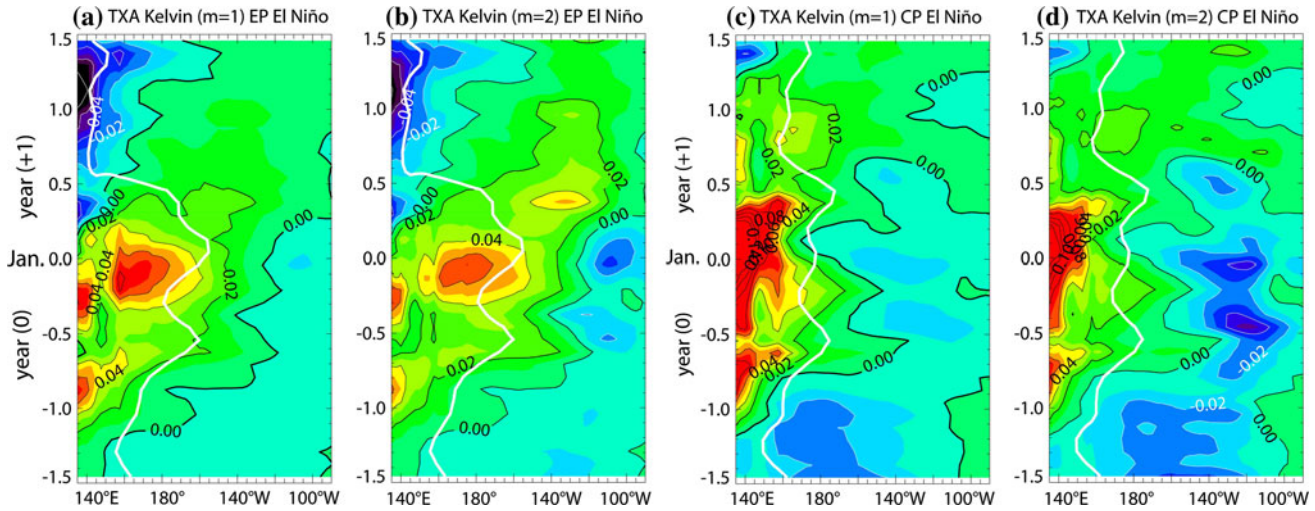

Fig. 11 Time longitude section of the zonal wind stress anomalies projected onto the Kelvin waves for the first (**a–c**) and second (**b–d**) baroclinic modes for EP (**a–b**) and CP (**c–d**) El Niños. The *thick white line* represents the position of the 28°C isotherm for SST

maximum at this longitude of the variability of the second baroclinic mode Kelvin wave (Fig. 8c).

In order to estimate to which extent the characteristics of the wind stress forcing during the two El Niño types are influential on the Kelvin wave characteristics, the zonal wind stress anomalies projected onto the Kelvin wave was estimated for the first two baroclinic modes (Fig. 11). The zonally varying wind projection coefficient was used to take into account the fact that the second mode has more energy in the eastern Pacific (due to the shallower thermocline). Interestingly, it indicates that easterlies have developed during the development of the CP El Niño in the central-eastern Pacific and that those project preferentially on the second baroclinic mode (Fig. 11d, Year −0.5 and Year 0). These however have no clear counterpart in the Kelvin wave contribution to sea level anomalies (Fig. 8c), which suggests the presence of compensating downwelling Kelvin wave in the eastern Pacific resulting from the modal dispersion of the energetic first baroclinic mode (Fig. 8a) towards the second baroclinic mode. On the other hand, during the decaying phase an upwelling Kelvin wave of the second baroclinic mode is present without any evidence of energetic easterlies projecting on the second baroclinic mode (Fig. 8c, Year +1). This upwelling wave apparently originates from the western Pacific suggesting that it results from the reflection of a Rossby wave at the western boundary. The increase in amplitude of this wave during its propagation (especially around 140°W) has to result from modal dispersion associated to the sloping thermocline. This further indicates that the delayed oscillator mechanism is operating during the CP El Niño through the second baroclinic mode, consistently with the evolution of the WWV of the second baroclinic mode evidenced in Fig. 10b.

Summarizing the difference between CP and EP El Niño events in terms of equatorial wave dynamics, our results suggest that during CP El Niño, there is a decoupling between baroclinic modes: The first mode drives the ocean basin mode (Neelin and Jin 1993; Kang et al. 2004) and participate to the recharge process, whereas the second mode is associated to the delayed oscillator mechanism and participates to the discharge process. For the EP El Niño, despites difference in the amplitude and phasing of the baroclinic modes, both modes have a comparable role in the recharge-discharge process. This has clear implication for the understanding of the characteristics of the CP El Niño (amplitude, frequency, duration and propagating characteristics).

We now discuss limitations of our study. First of all, although the GFDL model has been shown to be skillful in simulating many aspects of the ENSO variability (Wittenberg et al. 2006; Capotondi et al. 2006; Kug et al. 2009), it has a tendency to simulate patterns of tropical Pacific SST, wind stress, and precipitation variability too much to the west. This in particular may lead to an unrealistic simulation of the ENSO feedback processes. For instance, a wind stress forcing located to close to the western boundary does not allow for accumulation of momentum forcing towards the upwelling Rossby wave, nor does it allow for the delayed oscillator process resulting from the out of phase relationship between the forced downwelling Kelvin wave and the reflected upwelling Kelvin wave. The centre of action of the wind stress anomaly also determines the balance between the zonal-advective and thermocline feedbacks, and so the ENSO stability (An and Jin 2001). In particular a location too much to the west of the wind stress anomaly will tend to favour the zonal-advective feedback and so the near-annual Pacific basin mode (Kang et al.

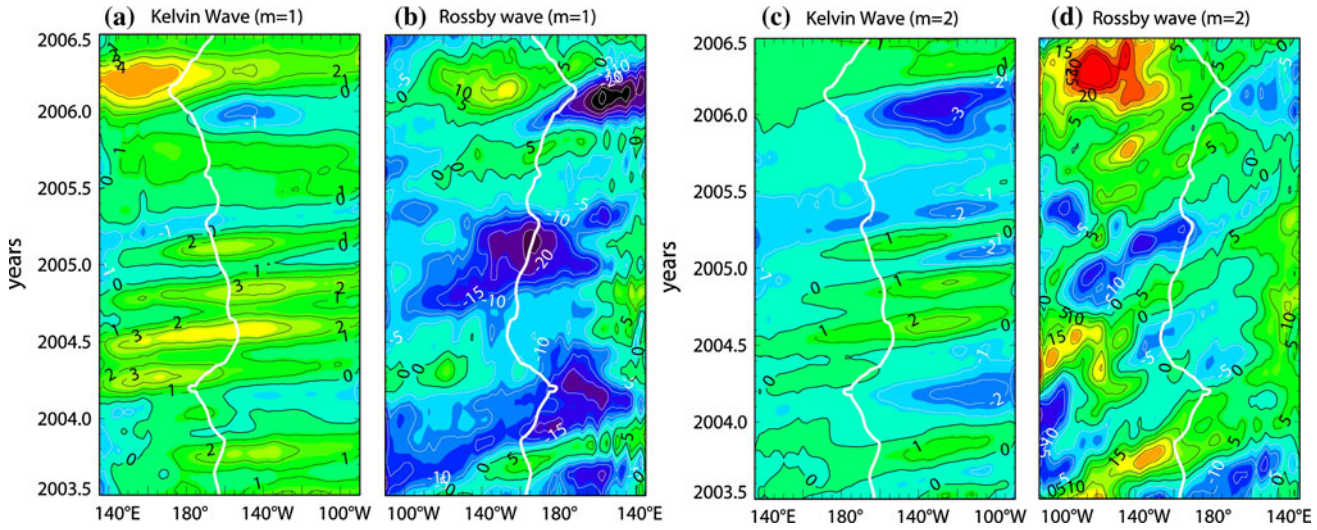

Fig. 12 Same as Fig. 8 but for the SODA Reanalysis and for the 2004/2005 Modoki El Niño. Anomalies are relative to the mean seasonal cycle computed over the period 1958–2008

2004). This is consistent with the results of the wave decomposition which clearly shows the basin mode nature of the first baroclinic mode during periods of high CP El Niño (Fig. 8a). In the observations, the wind stress anomaly associated to ENSO is not as much to the west as in the GFDL model. However, during observed CP El Niños, it is somewhat $\sim 10°$ to the west of that during EP El Niños and does not extent as much to the east (not shown). This has the potential to modify the balance between the feedback processes in a way that may also favour the near-annual Pacific basin mode. Nevertheless composite analysis based on the new ocean reanalysis (SODA) that covers the period from 1871 to 2008 (Giese and Ray 2011) does not reveal a contrasted behaviour between both type of El Niño in terms of their vertical structure variability. The SODA CP composite[1] for the first baroclinic mode do exhibit pulses of downwelling Kelvin wave peaking in the central Pacific and having decaying amplitude near the boundaries reminiscent of the ocean basin mode (not shown). However both baroclinic modes are characterized by a clear reversal from warm to cold indicating that they have comparable behaviour of the discharge process, conversely to the GFDL CP composite. It is difficult here to draw firm conclusions from the SODA composite due to the sensitivity of the results to the number of event that are retained. It is clear that there is a larger diversity of the evolution of the events in the SODA Reanalysis compared to the GFDL model, which somehow limits any generalisation. In particular, Kug et al. (2009) introduced three types of El Niño, i.e. CP, EP, and a mixed type. For instance, the last El Niño to date that took place in 2009–2010 can be categorized as a CP El Niño (Kim et al. 2011) but its ocean dynamical behavior resembles the EP El Niño. Yu et al. (2011) also propose to define CP El Niño and mixed-type El Niño based on subsurface indices that are more appropriate to capture the specificities of the events and account for the larger diversity of the El Niño types in nature than what is simulated in the GFDL model. Noteworthy the GFDL model is also characterized by a clear relationship between mean state and CP El Niño occurrence (Choi et al. 2011) which is not evidenced from the SODA reanalysis. In fact, the increased occurrence of the CP El Niño occurs under a warmer mean state in the central Pacific in the GFDL model, which somehow is comparable to the situation in the recent decade (Takahashi et al. 2011; McPhaden et al. 2011). It is then likely that CP El Niños that occurred during the last decade (2000–2010) are more comparable to the GFDL CP El Niño. As a consistency check of this later statement, we diagnosed the Kelvin and Rossby waves in the SODA Reanalysis for the 2004/2005 El Niño (Fig. 12). It indicates that the vertical structure variability of the 2004/2005 El Niño is qualitatively comparable to the GFDL CP composite, with in particular the first (second) baroclinic more contributing more to the warming (cooling) of SST during its cycle.

Besides limitations associated to model biases, it is worth mentioning the one limitation associated to the compositing procedure from monthly-mean outputs that tends to damp high-frequency variability potentially having a critical role on the development and evolution of the CP El Niño. As a matter of fact, since the convection zone remains "trapped" around the mean position of the warm pool, equatorial convective atmospheric waves and associated westerly wind bursts are favoured during all the phases of the event. In particular, at year (+1), while the

[1] Over this period, 20 CP can be selected based on the definition of Yeh et al. (2009).

EP El Niño event starts its decaying phase (and its reversal to cool conditions), the warm conditions during the CP El Niño can be maintained by the convective equatorial wave activity at the consecutive peak season (March–April–May). This stresses on the likely stronger coupling between tropical intraseasonal atmospheric variability and ENSO during the CP El Niño than during the EP El Niño. Current efforts are devoted to the investigation of such aspect of the CP and EP El Niño variability.

Acknowledgments S.-I. An was supported by the National Research Foundation of Korea (NRF) grant funded by the Korea government (MEST) (No. 2011-0015208). Sulian Thual benefited from support of the CNRS (Centre National de la Recherche Scientifique) through a STAR (Science and Technology Amicable Research) program (No. 25848VL). The two anonymous reviewers are thanked for their constructive comments.

References

An S-I, Jin F–F (2000) An eigen analysis of the interdecadal changes in the structure and frequency of ENSO mode. Geophys Res Lett 27:1573–1576

An S-I, Jin F–F (2001) Collective role of thermocline and zonal advective feedbacks in the ENSO mode. J Clim 14:3421–3432

Ashok K, Behera SK, Rao SA, Weng H, Yamagata T (2007) El Niño Modoki and its possible teleconnection. J Geophys Res 112:C11007

Bejarano L, Jin F–F (2008) Coexistence of equatorial coupled modes of ENSO. J Clim 21:3051–3067

Blumenthal B, Cane MA (1989) Accounting for parameter uncertainties in model verification: an illustration with tropical sea surface temperature. J Phys Oceanogr 19:815–830

Boulanger J-P, Menkes C (1999) Long equatorial wave reflection in the Pacific Ocean during the 1992–1998 TOPEX/POSEIDON period. Clim Dyn 15:205–225

Busalacchi AJ, Cane MA (1988) The effect of varying stratification on low-frequency equatorial motions. J Phys Oceanogr 18(6):801–812

Capotondi A, Wittenberg A, Masina S (2006) Spatial and temporal structure of tropical Pacific interannual variability in 20th century coupled simulations. Ocean Model 15:274–298

Carton JA, Giese BS (2008) A reanalysis of ocean climate using simple ocean data assimilation (SODA). Month Weath Rev 136(8):2999–3017

Choi J, An S-I, Kug J-S, Yeh S-W (2011) The role of mean state on changes in El Niño's flavours. Clim Dyn 37:1205–1215

Cravatte S, Delcroix T, Zhang D, McPhaden M, Leloup J (2009) Observed freshening and warming of the western Pacific warm pool. Clim Dyn 33:565–589. doi:10.1007/s00382-009-0526-7

Delworth TL et al (2006) GFDL's CM2 global coupled climate models. Part I: formulation and simulation characteristics. J Clim 19:634–674

Dewitte B (2000) Sensitivity of an intermediate coupled ocean-atmosphere model of the tropical Pacific to its oceanic vertical structure. J Clim 13:2363–2388

Dewitte B, Reverdin G, Maes C (1999) Vertical structure of an OGCM simulation of the equatorial Pacific Ocean in 1985–1994. J Phys Oceanogr 29:1542–1570

Dewitte B, Illig S, Parent L, duPenhoat Y, Gourdeau L, Verron J (2003) Tropical Pacific baroclinic mode contribution and associated long waves for the 1994–1999 period from an assimilation experiment with altimetric data. J Geophys Res 108(C4):3121–3138

Dewitte B, Yeh S-W, Moon B-K, Cibot C, Terray L (2007) Rectification of the ENSO variability by interdecadal changes in the equatorial background mean state in a CGCM simulation. J Climate 20(10):2002–2021

Dewitte B, Thual S, Yeh S-W, An S-I, Moon B-K, Giese B (2009) Low frequency variability of temperature in the vicinity of the equatorial thermocline in SODA: role of equatorial wave dynamics and ENSO asymmetry. J Climate 22:5783–5795

Giese B, Ray S (2011) El Niño variability in simple ocean data assimilation (SODA):1871–2008. J Geophys Res 116:C02024. doi:10.1029/2010JC006695

Gnanadesikan A et al (2006) GFDL's CM2 global coupled climate models, Part II: the baseline ocean simulation. J Clim 19:675–697

Griffies SM et al (2005) Formulation of an ocean model for global climate simulations. Ocean Sci 1:45–79

Jin FF (1997) An equatorial ocean recharge paradigm for ENSO. Part I: conceptual model. J Atmos Sci 54:811–829

Jin F–F, Neelin JD (1993) Modes of interannual tropical ocean-atmosphere interaction—a unified view. Part I: numerical results. J Atmos Sci 50:3477–3503

Jin F-F, Kug JS, An S-I, Kang IS (2003) A near-annual coupled ocean-atmosphere mode in the equatorial Pacific Ocean. Geophys Res Lett 30:1080. doi:10.1029/2002GL015983

Kang I-S, Kug J-S, An S-I, Jin F–F (2004) A near-annual Pacific Ocean Basin mode. J Clim 17:2478–2488

Kao H-Y, Yu J-Y (2009) Contrasting Eastern-Pacific and Central-Pacific types of ENSO. J Clim 22:615–632

Kim W, Yeh S-W, Kim J-H, Kug J-S, Kwon M (2011) The unique 2009–2010 El Niño event: a fast phase transition of warm pool El Niño to La Niña. Geophys Res Lett 38:L15809. doi:10.1029/2011GL048521

Kug J-S, Kang I-S, An S-I (2003) Symmetric and asymmetric mass exchanges between the equatorial and off-equatorial Pacific associated with ENSO. J Geophys Res 108(NO. C8):3284. doi:10.1029/2002JC001671

Kug J-S, Jin F–F, An S-I (2009) Two-types of El Niño events: cold Tongue El Niño and Warm Pool El Niño. J Clim 22:1499–1515

Kug J-S, Choi J, An S-I, Jin F–F, Wittenberg A-T (2010) Warm pool and cold tongue El Nino events as simulated by the GFDL2.1 coupled GCM. J Clim 23:1226–1239

Larkin NK, Harrison DE (2005a) On the definition of El Niño and associated seasonal average U.S. weather anomalies. Geophys Res Lett 32:L13705

Larkin NK, Harrison DE (2005b) Global seasonal temperature and precipitation anomalies during El Niño autumn and winter. Geophys Res Lett 32:L16705

Lee T, McPhaden M (2010) Increasing intensity of El Nino in the central-equatorial Pacific. Geophys Res Lett 37:L14603. doi:10.1029/2010GL044007

Lighthill MJ (1969) Dynamical response of the Indian Ocean to onset of the southwest monsoon. Phil Trans R Soc A 265:45–92

Lin S-J (2004) A "vertically Lagrangian" finite-volume dynamical core for global models. Mon Wea Rev 132:2293–2307

McPhaden MJ (2004) Evolution of the 2002–03 El Niño. Bull Am Meteor Soc 85:677–695

McPhaden MJ, Busalacchi AJ, Cheney R, Donguy JR, Gage KS, Halpern D, Ji M, Julian P, Meyers G, Mitchum GT, Niiler PP, Picaut J, Reynolds RW, Smith N, Takeuchi K (1998) The tropical ocean-global atmosphere (TOGA) observing system: a decade of progress. J Geophys Res 103:14169–14240

McPhaden MJ, Lee T, McClurg D (2011) El Niño and its relationship to changing background conditions in the tropical Pacific Ocean. Geophys Res Lett 38:L15709. doi:10.1029/2011GL048275

Meinen CS, McPhaden MJ (2000) Observations of warm water volume changes in the equatorial Pacific and their relationship to El Niño and La Niña. J Clim 13:3551–3559

Neelin JD, Jin F–F (1993) Modes of interannual tropical ocean–atmosphere interaction—a unified view. Part II: analytical results in the weak-coupling limit. J Atmos Sci 50:3504–3522

Neelin JD, Battisti DS, Hirst AC, Jin F–F, Wakata Y, Yamagata T, Zebiak SE (1998) ENSO theory. J Geophy Res Oceans 103:14261–14290

Picaut J, Ioualalen M, Menkes C, Delcroix T, McPhaden MJ (1996) Mechanism of the Zonal displacements of the pacific warm pool: implications for ENSO. Science 274:1486–1489

Schopf P-S, Suarez M-J (1988) Vacillations in a coupled ocean-atmosphere model. J Atmos Sci 45:549–566

Suarez MJ, Schopf PS (1989) A delayed action oscillator for ENSO. J Atmos Sci 45:3283–3287

Takahashi K, Montecinos A, Goubanova K, Dewitte B (2011) ENSO regimes: reinterpreting the canonical and Modoki El Niño. Geophys Res Lett 38:L10704. doi:10.1029/2011GL047364

Weng H, Ashok K, Behera S, Rao S, Yamagata T (2007) Impacts of recent El Niño Modoki on dry/wet conditions in the Pacific Rim during boreal summer. Clim Dyn 29:113–129

Wittenberg A, Rosati TA, Lau N-C, Ploshay JJ (2006) GFDL's CM2 global coupled climate models. Part III: tropical Pacific climate and ENSO. J Clim 19:698–722

Yeh S-W, Kug S-J, Dewitte B, Kwon M-H, Kirtman BP, Jin F–F (2009) El Niño in a changing climate. Nature 461:511–514

Yu J-Y, Kim ST (2010a) Three evolution patterns of Central-Pacific El Niño. Geophys Res Lett 37:L08706. doi:10.1029/2010GL042810

Yu J-Y, Kim ST (2010b) Identification of Central-Pacific and Eastern-Pacific types of ENSO in CMIP3 models. Geophys Res Lett 37. doi:10.1029/2010GL044082

Yu J-Y, Kim ST (2011) Relationships between extratropical sea level pressure variations and the Central Pacific and Eastern Pacific types of ENSO. J Clim 24:708–720

Yu J-Y, Kao H-Y, Lee T (2010) Subtropics-related interannual sea surface temperature variability in the central equatorial Pacific. J Clim 23:2869–2884

Yu J-Y, Kao H-Y, Lee T, Kim S (2011) Subsurface ocean temperature indices for Central-Pacific and Eastern-Pacific types of El Niño and La Niña events. Theoretical Appl Climatol 103:337–344

Zelle H, Appeldoorn G, Burgers G, van Oldenborgh GJ (2004) The relationship between sea surface temperature and thermocline depth in the eastern equatorial Pacific. J Clim 34:643–655